Understanding disruptions in tokamaks

Leonid E. Zakharov, Sergei A. Galkin, Sergei N. Gerasimov, and JET-EFDA contributors

Citation: Phys. Plasmas **19**, 055703 (2012); doi: 10.1063/1.4705694
View online: http://dx.doi.org/10.1063/1.4705694
View Table of Contents: http://pop.aip.org/resource/1/PHPAEN/v19/i5
Published by the American Institute of Physics.

Understanding disruptions in tokamaks[a)]

Leonid E. Zakharov,[1,b)] Sergei A. Galkin,[2] Sergei N. Gerasimov,[3] and JET-EFDA contributors[3,c)]
[1]*PPPL, Princeton University, Princeton, New Jersey 08543, USA*
[2]*FAR-TECH, Inc., 10350 Science Center Dr. Bld. 14, St 150, San Diego, California 92121, USA*
[3]*EURATOM/CCFE Fusion Association, Culham Science Centre, Abingdon, Oxfordshire OX14 3DB, United Kingdom*

(Received 20 January 2012; accepted 19 March 2012; published online 1 May 2012)

This paper describes progress achieved since 2007 in understanding disruptions in tokamaks, when the effect of plasma current sharing with the wall was introduced into theory. As a result, the toroidal asymmetry of the plasma current measurements during vertical disruption event (VDE) on the Joint European Torus was explained. A new kind of plasma equilibria and mode coupling was introduced into theory, which can explain the duration of the external kink 1/1 mode during VDE. The paper presents first results of numerical simulations using a free boundary plasma model, relevant to disruptions. [http://dx.doi.org/10.1063/1.4705694]

I. INTRODUCTION

The tokamak concept is based on Shafranov's stability criterion[1,2] for the free boundary kink modes. His initial model was an ideally conducting plasma column (with a circular cross-section) in a strong magnetic field with a vacuum region outside. Although the basic stability requirement of a strong magnetic field (or plasma current limitations) and criterion $q(a) > 1$ ($q(\rho) \equiv \rho B_\phi / R B_\omega$, $\rho, \omega, R\phi$ are cylindrical coordinates, a, R are the minor and major radii of the plasma, B_ϕ, B_ω are toroidal and poloidal magnetic fields) have been confirmed by the first tokamak experiments, the plasma could be macroscopically unstable even at higher q_a than expected based on the original stability condition. Later on it was understood, that the safety factor $q(0)$ in the plasma center is limited by internal reconnections,[3,4] which elevated the theoretical requirements for the edge value of q_a to $q_a > 2$.[5] Following progress in plasma heating the theory of the free boundary kink mode was complemented by finite plasma pressure effects.[6]

In this paper, the finite pressure effects are not considered. Even without additional complications related to them, the macroscopic stability of a low pressure plasma does not follow precisely the ideal stability conditions. Thus, in tokamaks, the criterion $q_a > 2$ cannot be approached: magnetohydrodynamic (MHD) instabilities in the form of disruptions terminate the discharge.

The first publication about disruptive instability[7] in tokamaks appeared in 1963. Even at this early stage of tokamak research, it was noticed that plasma-wall interaction plays a significant role during disruptions. This indicated that the Shafranov free boundary kink mode model is only approximate.

The most significant apparent deviation from the free boundary plasma model (a plasma core inside closed magnetic surfaces and vacuum outside them) came in 1991 from DIII-D measurements[8] of the currents to the plasma facing surface of carbon tiles during vertical instability. Surprisingly, the currents to the tile surface were measured far away from the contact zone of the plasma with the tiles. In accordance with magnetic reconstruction by EFIT,[9] the interpretation was that the currents to the tiles surface are flowing from the open field lines outside the plasma core. The existence of these, so-called "halo" currents, was not taken into account by the Shafranov free boundary model. Then, the tile current diagnostics were improved and extended to a full toroidal angle by Evans,[10] thus, allowing measurements of asymmetries in the scrape off layer currents. During vertical disruption event (VDE), the toroidal asymmetry and rotation of the tile currents have been observed on JT-60U,[11] Cmod,[12] DIII-D,[13] indicating the presence of a kink mode during vertical instability. Since that time, tile current diagnostics have been installed on numerous tokamaks and contributed to the paradigm of the halo currents and associated notion of the toroidal peaking factor as a measure of their asymmetry. Later on, theory papers[14] relying on the halo current picture explained the dependence of the toroidal peaking factor as a function of the total halo current.

Separately from the tile current measurements, beginning in 1995, a significant toroidal asymmetry in the plasma current measurements was observed on Joint European Torus (JET) (Refs. 15 and 16) during VDE, manifesting another deviation from the free boundary plasma model. Even, without direct tile current measurements, this asymmetry indicated that some current is flowing from the plasma volume to the wall. The magnetic diagnostics, situated inside the wall surface, do not detect these currents and, as a result, the plasma current reconstructed from the internal magnetic measurements appears to be different in different toroidal cross-sections.

At first glance, JET data simply complement the picture of the halo currents. In fact, as it was shown in Ref. 17, they significantly undermined it. It was shown that the theory based on Shafranov's free boundary plasma, when complemented by the plasma-wall current sharing effect (Hiro

[a)]Paper VI3 2, Bull. Am. Phys. Soc. **56**, 356 (2011).
[b)]Invited speaker.
[c)]See the Appendix of F. Romanelli *et al.*, Proceedings of the 23rd IAEA Fusion Energy Conference 2010, Daejeon, Korea.

currents), explains the sign of the wall currents in JET measurements, while the widely adopted concept of the halo currents is in a clear contradiction with the sign of measurements.

This paper describes the profound effect of rehabilitation of the free boundary plasma model on understanding and simulations of the vertical disruption events. VDEs represent the simplest but the most dangerous type of disruptions regarding the forces on the vessel and in-vessel components of tokamaks. Better understanding of VDEs, including the associated $m/n=1/1$ kink mode, and the current sharing effect, which is the primary focus of the paper, should have an impact on understanding of other types of disruptions where plasma contacts the wall at the earliest phase (m, n are poloidal and toroidal wave numbers).

Section II describes the surface currents during free boundary instabilities. Sections III–V explain the difference between the Hiro currents and eddy currents, the specifics of magnetic measurements during instabilities, forces to the wall, the wall touching kink mode (WTKM), and associated new type of plasma equilibria and the mode coupling.

Section VI specifies requirements for disruption simulations schemes and outlines the approach adopted by a disruption simulation code (DSC) development. Its operational 2-D version based on the Shafranov model is used for illustrations. They include two plasma regimes with Hiro currents, relevant to disruptions, which cannot be reproduced by other codes because of their incorrect restriction $V_{normal}=0$ on the plasma velocity into the wall. The requirements for disruption simulation schemes are outlined together with the approach adopted by a DSC development.

Section VII suggests an alternative, based on the theory of WTKM, interpretation of the currents to the tile surface, in contrast to the currently adopted halo current concept. The paper is concluded by a summary (Sec. VIII).

II. PHYSICS OF SURFACE CURRENT GENERATION

The basic physics of kink modes can be explained using a cylindrical (single helicity mode) model of a plasma with a circular cross-section in a strong longitudinal magnetic field. In fact, the strongest kink mode $m/n=1/1$ represents the easiest example for the theory analysis as well as the focus of the recent ITER interest because of resulting large sideways forces on the vacuum vessel.[16]

During the kink instability, the plasma surface exhibits a helical deformation

$$\rho = a + \xi_{mn}\cos(m\omega - n\phi). \tag{1}$$

Neglecting plasma inertia, the plasma surface represents a magnetic flux surface, essentially independent of plasma resistivity. In order to eliminate the normal component B_{normal} of the magnetic field, the plasma generates surface currents. Their formal linear theory is described in Refs. 5, 17–19, while a non-linear analysis requires numerical simulations.

For the $m/n=1/1$ kink mode in the absence of a conducting wall, the surface current $\vec{\imath}_{11}^{surf}$ can be calculated from the condition $B_{normal}=0$ as (SI units are used)

$$\mu_0\vec{\imath}_{11}^{surf} = -2\xi_{11}\frac{B_\phi}{R}\left(\vec{e}_\phi + \frac{a}{R}\vec{e}_\omega\right)\cos(\omega-\phi),$$
$$\mu_0 \equiv 0.4\pi\cdot 10^{-6}. \tag{2}$$

The remarkable facts are that the value of the surface current

- does not contain the resonant factor $m/n-q_a=1-q_a$ and
- is determined by the plasma displacement and deformation, rather than by plasma velocity.

The first property determines the large amplitude of $\vec{\imath}_{11}^{surf}$ and makes it present at the plasma edge even when q_a crosses its resonant value $q_a=m/n$ and the plasma becomes unstable. The second property is even more substantial. It means that the kink instability acts as a current, rather than a voltage, generator for the surface current.

The finite inertia effects on the surface and edge currents were considered in Refs. 18–20. They lead to generation of the poloidal component of the surface currents, compensating the jump in the kinetic and magnetic field pressure across the plasma edge. The poloidal component of the surface currents is supplied by a radial current from the plasma core. As was noticed by Webster,[18] they make the total surface current force-free. The poloidal surface currents do not affect the magnetic configuration and their role (if any) in disruptions is not yet revealed. In the simulations presented in this paper, they are taken into account automatically.

Here we advance the theory of the above references with explanation of the physics mechanism of excitation of surface currents. At the plasma edge, Ampère's law for the surface current can be written as

$$-\frac{\partial\vec{A}}{\partial t} + \vec{V}\times\vec{B} - \nabla_{surf}\phi_E = \frac{\vec{J}^{edge}}{\sigma}, \tag{3}$$

where $\vec{A},\vec{V},\vec{B},\phi_E$ are the vector potential, plasma velocity at the edge, magnetic field, and electric scalar potential, while $\vec{j}^{edge},\sigma$ are the current density and electric conductivity in the actual layer of surface current localization. In terms of components and separate sources, this equation can be written as

$$-\frac{\partial\vec{A}^{i,surf}}{\partial t} - \underbrace{\frac{\partial\vec{A}^{pl,core}}{\partial t} + V_{normal}B_\omega\vec{e}_\phi}_{vanishes\ for\ m=1}$$
$$-\underbrace{V_{normal}B_\phi\vec{e}_\omega}_{driving\ EMF} - \nabla_{surf}\phi_E = \frac{\vec{j}^{edge}}{\sigma}. \tag{4}$$

The superscripts "*surf*", and "*core*" have the obvious meaning. Because for the $m=1$ displacement the magnetic field of the core current moves together with the plasma cross-section, the core does not contribute to Ampère's law.

As a result, the driving electromotive term becomes evident: the surface currents of the kink mode are generated by the plasma motion in the *toroidal* magnetic field. Because the value of $\vec{\imath}^{surf}$ is determined by the plasma deformation ξ, Ampère's law (4) serves as an equation for determining

plasma velocity V_{normal} rather than, as it would be in electrodynamics, for calculating the surface current density, given the velocity. This understanding of causality is important for developing numerical schemes for kink mode simulations.

Fig. 1(a) explains the balance between the driving term and the scalar electric field $\nabla_{surf}\phi_E$. In this case, the $q_a < 1$ and the magnetic field lines have a steeper angle than the line $\omega = \phi$ corresponding to the ignorable direction $\mathbf{e}_\phi + a/R\mathbf{e}_\omega$ for the $m/n = 1/1$ mode.

The $\nabla_{surf}\phi_E$ term compensates the perpendicular to the ignorable direction projection of the driving $V_{normal}B_\phi\vec{e}_\omega$ term. The remaining uncompensated component represents the electro-motive force EMF

$$\vec{EMF} = \frac{a}{R}V_{normal}B_\phi\left(\mathbf{e}_\phi + \frac{a}{R}\mathbf{e}_\omega\right). \tag{5}$$

The physics of the surface currents is similar for all $m \geq 1$ kink modes. The major difference is that for the $m > 1$ kink modes, there is no complete compensation of the core perturbation in Ampère's law and the value of the surface currents is typically smaller than for the special $m/n = 1/1$ case. The two important above mentioned properties of the surface currents remain valid for all kink modes.

It is important to realize that the basic elements of the physics of the kink modes have their analog also in the vertical instability $m/n = 1/0$ of an elongated plasma. Because of its axial symmetry $n = 0$, this instability is typically simulated using equilibrium codes (e.g., DINA (Refs. 21 and 22)), which solve the Grad–Shafranov (GSh) equation. The TSC code[23] solves dynamical equations but it is not clear that it can resolve the surface currents generated by the instability.

In fact, the approach based solely on the GSh equation misses the physics of the surface currents, important for plasma dynamics in certain regimes. As is shown in Fig. 1(b), the plasma motion in the external field of poloidal field coils (PF coils) creates the electro-motive force generating the surface currents. In the case of vertical instability, corresponding Ampère's law can be reduced to

$$-\frac{\partial\vec{A}^{i,surf}}{\partial t} + \underbrace{\vec{V}\times\vec{B}^{PFC}}_{Driving\ EMF} = \frac{\vec{j}^{surf}}{\sigma}. \tag{6}$$

As for the $m/n = 1/1$ kink mode, the contribution from interaction of the plasma motion with its own magnetic field vanishes together with $-\nabla_{surf}\phi_E = 0$, and the remaining driving term represents the EMF

$$\vec{EMF} = \vec{V}\times\vec{B}^{PFC}. \tag{7}$$

For a plasma with a uniform current core j and elliptical cross-section,

$$x \equiv r - R = a\cos\theta, \quad z = \kappa a\sin\theta, \tag{8}$$

where r is the major radius of a tokamaks cylindrical coordinates r, ϕ, z, and κ is the plasma ellipticity, the expression for the surface current $i_{10}^{surf}\mathbf{e}_\phi$ can be derived analytically using the formalism of review[24]

$$i_{10}^{surf} = -j\frac{\kappa(\kappa-1)}{\kappa^2+1}\frac{\xi\sin\theta}{\sqrt{1+(\kappa^2-1)\cos^2\theta}}, \tag{9}$$

where ξ_{10} represents the plasma vertical displacement. Without presenting here a fairly straightforward derivation, the equation of plasma motion can be written as

$$\mu_0\rho_{pl}\frac{d^2\xi_{10}}{dt^2} = \frac{\mu_0^2 j^2\kappa}{(\kappa^2+1)^2}\sqrt{\frac{\kappa-1}{\kappa+1}}\xi, \tag{10}$$

where $\rho_{pl} = nm_i$ is the plasma density.

It is remarkable that both Eqs. (9) and (10) describe the exact nonlinear analytical solution for vertical instability of the plasma with an elliptical cross-section and a uniform

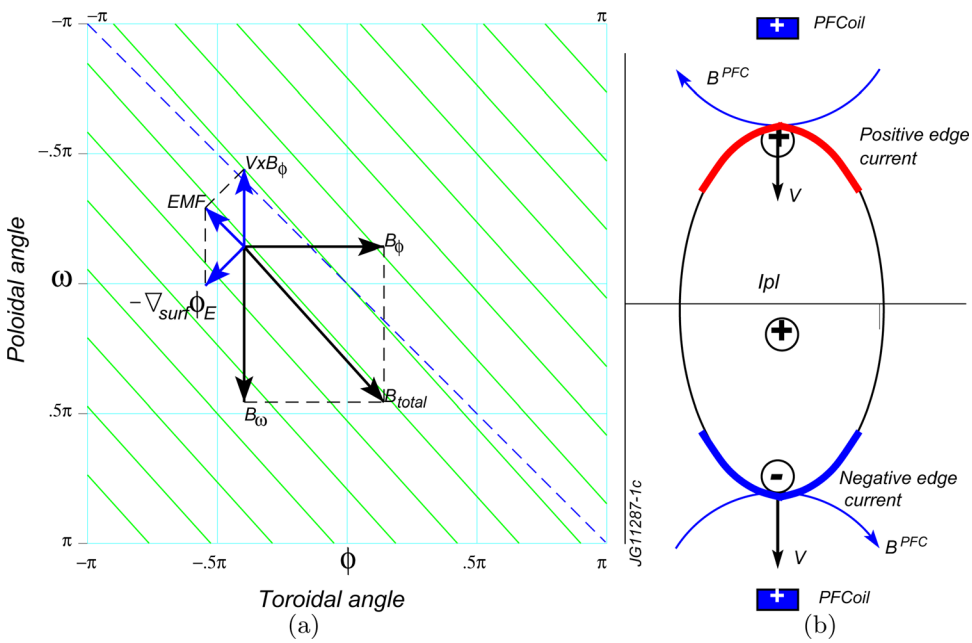

FIG. 1. (a) $\phi - \omega$ plane representing the plasma surface, the dashed line represents the ignorable direction for the single helicity $m/n = 1/1$ kink perturbation and (b) elongated plasma cross-section moving from equilibrium position by vertical instability in the external field of the shaping poloidal field coils.

core current density. Magnetic configurations of three stages of this instability are shown in Fig. 2. As in the case of the kink mode, the surface currents are negative with respect to the plasma core current on the side of the plasma moving toward the wall. They can significantly modify the magnetic configurations in the vicinity of the initial X-point of the separatrix.

The surface currents generated by the axisymmetric $n=0$ modes during vertical instability have common properties with the kink modes $n \neq 0$

- they are excited by the plasma motion in an external magnetic field ($\vec{V} \times \vec{B}^{PFC}$);
- their amplitude is determined by the plasma displacement and deformation;
- the instability for them acts as current, rather than voltage, generator; and
- Ampère's law determines the plasma velocity given the current densities determined by the plasma dynamics.

Surface currents at the plasma edge represent the key feedback mechanism of tokamak plasma stability. Without them (as, e.g., in the case of liquid metals), the MHD configuration would be always unstable.

III. HIRO CURRENTS, WALL TOUCHING KINK MODE AND EDDY CURRENTS

A. Eddy currents

The above considered surface currents at the plasma boundary are excited by the plasma motion which is an MHD effect. In the presence of the wall, the perturbation of the magnetic field between the plasma and the wall excites eddy currents i^{eddy} in the wall and modifies the surface currents on the plasma. This is an electro-dynamic mechanism, different from MHD.

Returning to consideration of the kink modes, the perturbation of the normal component of magnetic fields $\tilde{B}_n$ in the vacuum region near the plasma boundary is related to the plasma displacement by

$$\tilde{B}_n = \vec{B} \cdot \nabla \xi, \quad \tilde{B}_{n,11} = \frac{B_\phi}{R} \frac{1-q_a}{q_a} \xi_{11}, \tag{11}$$

where $\vec{B}$ is the equilibrium magnetic field.

In the case of a circular cross-sections of the plasma and the wall, the eddy current for the $m/n=1/1$ kink mode can be calculated as

$$\mu_0 i_{11}^{eddy} = -\frac{1-q_a}{q_a} \frac{2\lambda}{1-\lambda} \frac{B_\phi \xi_{11}}{R}, \quad \lambda = \frac{a^2}{b^2}. \tag{12}$$

(Here, λ takes into account the effect of the wall.) Accordingly, the surface current at the plasma boundary is modified by an additional term equal in amplitude but opposite in sign to i^{eddy} current

$$\mu_0 i_{11}^{surf} = -2\frac{B_\phi \xi_{11}}{R} + \frac{1-q_a}{q_a} \frac{2\lambda}{1-\lambda} \frac{B_\phi \xi_{11}}{R} = -2\frac{B_\phi \xi_{11}}{R} - \mu_0 i_{11}^{eddy}. \tag{13}$$

The first term here provides the MHD equilibrium in the core, while the second screens the eddy current field. Note, that the two terms in expression for i^{surf} specify the left boundary of the instability zone, which for the $m/n=1/1$ mode is $\lambda < q_a < 1$.

The perturbation of the vacuum magnetic field due to plasma core motion is screened by the surface current, explaining the presence of the resonant factor $(1-q_a)$ in $\tilde{B}_{n,11}$ and in i_{11}^{eddy}. As a result, near the transition to the kink instability $q_a \to 1$, the eddy current i_{11}^{eddy} is much smaller than the plasma surface current and the stabilizing effect of the wall on plasma dynamics is negligible.

In the presence of an ideal wall, the free boundary kink mode (FBKM) can find its new non-linear equilibrium, which is maintained by the eddy currents. An example, calculated with an ideal MHD DSC code (see Sec. VI) is shown in Fig. 3. The unstable plasma with $q_a = 0.75$ (flat current density profile with $q(\rho) = 1$ in the core and a surface current, which makes $q_a < 1$), which mimics some aspects of

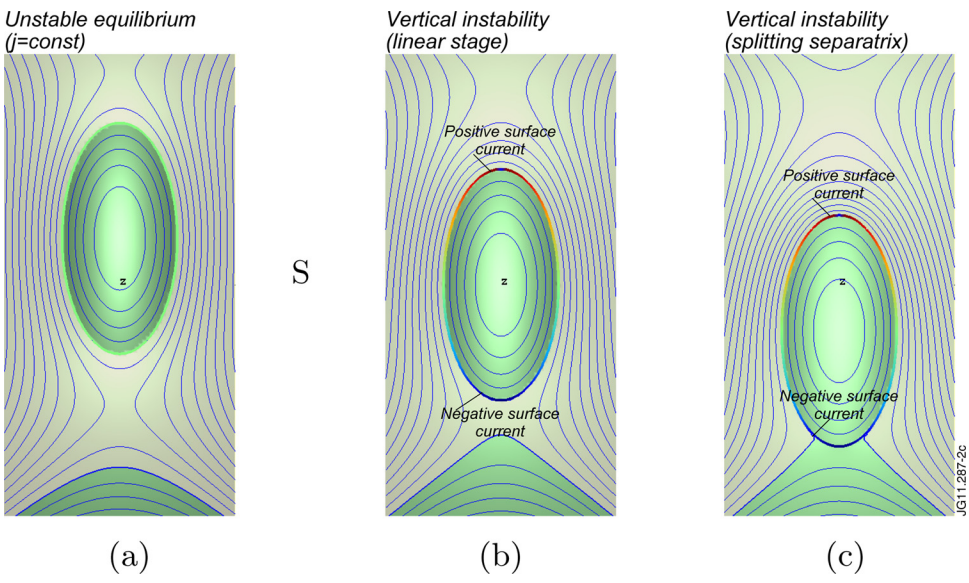

FIG. 2. Plasma vertical displacement, surface currents, and magnetic topology during vertical instability. (a) Initial (linear) displacement; (b) the intermediate stage with X-point of the separatrix approaching the plasma boundary; and (c) reversal of the poloidal magnetic field at the plasma boundary and splitting of the X-point.

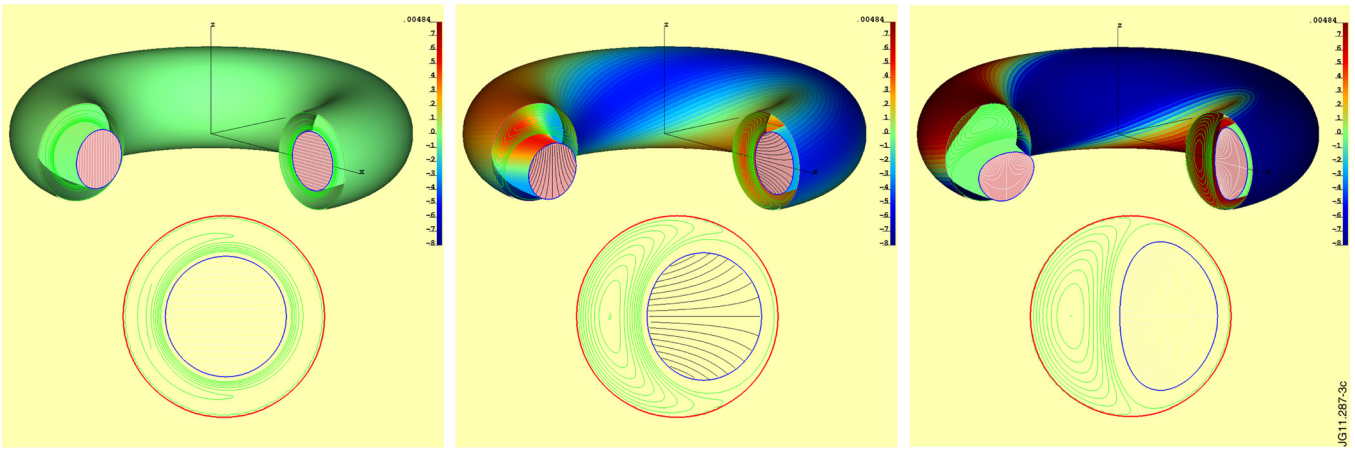

(a) (b) (c)

FIG. 3. Fast regime of the kink mode inside the ideal wall, both toroidal view and plasma cross-section are shown. (a) Initially perturbed plasma; (b) fast phase of instability (the blue lines in the core represent the flow function of plasma velocity); and (c) saturated state of the mode.

the kink mode during VDE, was initially displaced by a small $\xi_{11}\cos(\omega - \phi)$ perturbation. Then it moves toward the wall and the plasma shape exhibits deformation. In simulations, plasma inertia related oscillations were suppressed by introduction of an effective friction

$$\rho_{pl}\frac{d\vec{V}}{dt} \to \gamma\vec{V}, \tag{14}$$

where γ can be chosen as the linear growth rate of the mode. This substitution allows the plasma to reach a final equilibrium shown in Fig. 3(c).

During the plasma motion, both surface and eddy currents are excited. At the saturated state, the surface current on the plasma boundary loses its dipole character (angle dependence).

B. Hiro currents, WTKM, and JET disruption data

In reality, there are no ideally conducting walls. Also, multiple gaps, ribs, and penetrations make the electro-magnetically equivalent continuous wall different from the physical wall. Together with the finite resistivity, all "imperfections" of the wall facilitate the early contact of the plasma with the wall surface allowing current sharing between the plasma edge and the wall. This "galvanic" contact and associated WTKM, introduced in Ref. 17, represents a new effect in the disruption physics missed in previous theory, simulations, and interpretations of experiments.

The theory of WTKM suggests that the currents shared with the wall are the same surface currents which are excited by the instability and described earlier in this paper. In order to make clear distinction between them and the widely adopted concept of the "halo" currents along the open field lines, the instability driven currents were named "Hiro" currents.[17]

Then, the rigorous result of the theory is prediction of the negative sign (with respect to direction of the plasma current) of the Hiro currents shared with the wall, which is illustrated Fig. 4(a). In the fast MHD regime, Hiro currents are absolutely necessary for stabilizing the plasma. Unlike the

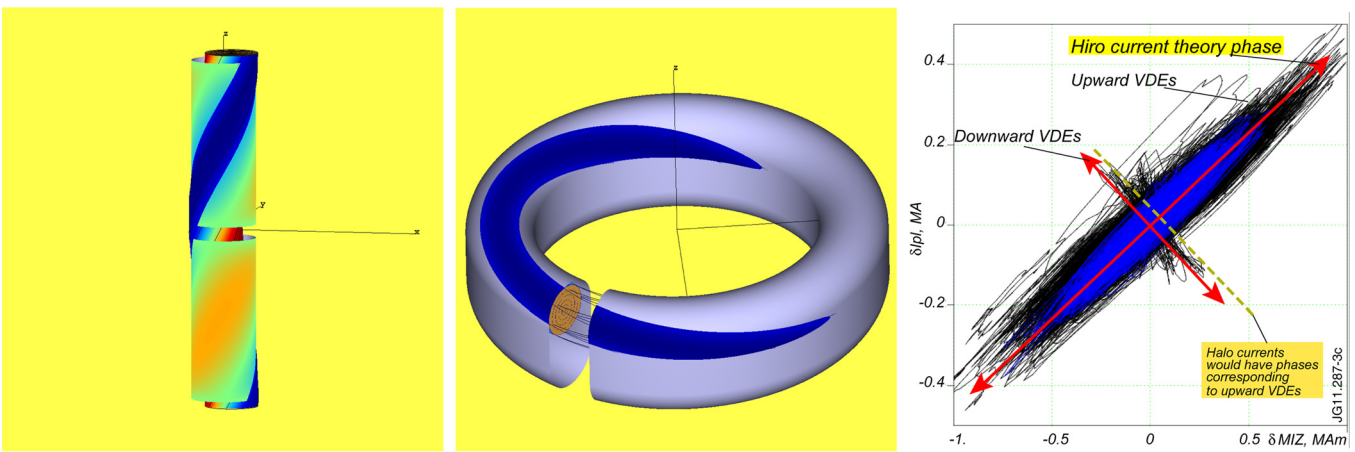

(a) (b) (c)

FIG. 4. Current sharing between plasma and the wall: (a) dark blue color represents the "Hiro" currents. (b) Toroidally localized "wetting" zone of the current sharing in VDE due to the WTKM $m/n = 1/1$. (c) Phase diagram of $I_{pl}(\phi + \pi, t) - I_{pl}(\phi, t)$ vs $M_{IZ}(\phi + \pi, t) - M_{IZ}(\phi, t)$ for all well diagnosed JET 4457 disruptions (as of August 2011).

eddy currents, Hiro currents are insensitive to the presence of gaps in the conducting surfaces. On the free plasma surface, they flow along the field lines.

The theory of WTKM automatically predicts toroidal asymmetry in the plasma current measurements, which was discovered in JET (Ref. 16) earlier. Fig. 4(b) shows that in tokamaks, the wall surface is not conformal to the plasma, and the wetting zone is toroidally localized. As a result, the internal magnetic measurements made under the wetting zone reconstruct a higher plasma current than those made where plasma does not touch the wall.

This predicted negative sign of the Hiro currents in the wall is in strong contrast with the widespread "halo"current (having opposite direction) interpretation of the wall currents and of the toroidal peaking factor (e.g., Ref. 14). Because of the importance of the controversy, the comprehensive list of disruptions with $I_{pl} > 1$ MA on JET during the 1994–2009 operation period was created (with the help of Mike Johnson) and a special code Cbdsr was written in 2009 for extraction and processing disruption data. Since 1994 for 3503 disruptive shots, the magnetic data are available from two octants 3,7 ($\phi_7 = 270^\circ, \phi_3 = 90^\circ$) and since 2005 for 954 disruptions from 4 octants, including additional octants 1,5 ($\phi_5 = 180^\circ, \phi_1 = 0^\circ$).

Fig. 4(c) shows the phase diagram[25] of toroidal asymmetries in measurements of the plasma current $\delta I_{pl}(t)$ and the so-called first vertical moment $\delta M_{IZ}(t)$

$$I_{pl}(\phi,t) \equiv \frac{1}{\mu_0}\oint B_\tau dl,$$
$$M_{IZ}(\phi,t) = \frac{1}{\mu_0}\oint\left[B_\tau z + (r^2 - R_0^2)B_n \ln\frac{r}{r_0}\right]dl \qquad (15)$$

made in opposite toroidal cross-sections $\phi_7 = 270^\circ, \phi_3 = 90^\circ$ (black curves) and $\phi_5 = 180^\circ, \phi_1 = 0^\circ$ (blue curves, activated in 2005)

$$\delta I(t) \equiv I_{pl}(\phi+\pi,t) - I_{pl}(\phi,t),$$
$$\delta M(t) \equiv M_{IZ}(\phi+\pi,t) - M_{IZ}(\phi,t). \qquad (16)$$

For both upward (about 1800 cases) and downward (20 cases) disruptions, the phase of asymmetry corresponds to the theory of WTKM and Hiro currents. All 4457 well diagnosed JET disruptive shots were processed.

Thus, the unique JET magnetic diagnostics activated in several toroidal cross-sections unambiguously dismisses the community-wide interpretation of asymmetric wall currents in VDE as halo currents. Below (see Sec. VII) the entire notion of "halo" currents (including their axisymmetric part) will be questioned.

IV. SIDEWAYS FORCES, MAGNETIC SIGNALS, AND PLASMA DISPLACEMENT

The understanding of disruptions became exceptionally important in relation with transition to the next step devices in which disruptions can damage the vessel structure. Thus, the energy (both poloidal magnetic W_M and thermal W_K) released in disruptions scales as

$$W_M \simeq \frac{1}{2}LI_{pl}^2 \propto I_{pl}^2 R, \quad W_K = \beta_{poloidal}W_M \propto W_M, \qquad (17)$$

where typical $\beta_{poloidal} \simeq 1$. Regarding the disruption problem, the step made earlier in the fusion program, from the DIII-D scale devices to JET corresponds to 7-fold enhancement in W_M

$$W_M^{JET} \simeq \left(\frac{3}{1.5}\right)^2 \cdot \frac{3}{1.7} \cdot W_M^{DIII-D} \simeq 7W_M^{DIII-D}, \qquad (18)$$

while W_M of the present next step, ITER device, corresponds to a big jump in the scaling coefficient relative to JET

$$W_M^{ITER} \simeq \left(\frac{15}{3}\right)^2 \cdot \left(\frac{6}{3}\right) W_M^{JET} \simeq 50W_M^{JET}. \qquad (19)$$

Accordingly vertical forces F_z in VDE and sideway forces F_x due to $m/n = 1/1$ kink mode on the vessel grow like

$$F_z \propto B^{PFC} I_{pl} R, \quad F_z^{ITER} \simeq 25F_z^{JET}, \quad F_x \propto B_\phi I_{pl} a,$$
$$F_x^{ITER} \simeq 20F_x^{JET}. \qquad (20)$$

Generation of runaway electrons (still tolerable at present) may grow to enormous proportions, i.e., to 10 MA/20 MeV in ITER, with the danger of releasing the energy in a localized manner.

Because of the large scale factors and new effects, the empirical approach based on accumulation of disruption data for a given device is no longer valid. In turn, the misinterpretation of existing disruption data (such as the halo current based one) can be fatal for the next step device operation.

A. Sideways forces in ITER

In this section, the sideways forces are considered as a result of development of the $m/n = 1/1$ kink mode during VDE. Originally, the sideways force acting on the plasma was assessed based on a simplistic model of a helically deformed conductor in a toroidal magnetic field[15]

$$F_x = \pi B_{tor} \cdot I_{pl} \cdot \xi_{11}. \qquad (21)$$

(Correct in scalings, this model does not reflect the properties of the tokamak plasma.) For practical use, the product $I_{pl} \cdot \xi_{11}$ was replaced by the measured M_{IZ} signal, thus, resulting in Noll's formula[16]

$$F_x^{Noll} = \pi B_{tor} \cdot \frac{\Delta M_{IZ}}{2}, \quad \Delta M_{IZ} \equiv M_{IZ}(\phi+\pi) - M_{IZ}(\phi). \qquad (22)$$

Because of quasi-static equilibrium, the same force should act on the wall. The beauty of the Noll formula is that it contains only directly measured information. Later on, Riccardo[26,27] suggested a "sink-source" model of wall currents by considering the potential circuits for the measured wall currents in the vessel structure. This consideration has effectively produced a similar estimate for F_x

$$F_x^{Riccardo} = \pi B_{tor} \cdot a \cdot \delta I_{pl} \simeq F_x^{Noll}, \qquad (23)$$

where one of the factors, i.e., the radial size a of the wall current circuit, was estimated as the radial semiaxis of the vessel rather than taken from measurements. Reflecting different aspects of asymmetry, both formulas give essentially the same force. In application to ITER, these formulas and analysis of sideways forces in a number of the most representative disruption shots on JET resulted in the design guidance at the level of $F_x^{ITER} \simeq 40 - 50$ MN.

Later on, using Cbdsr, the entire data base was processed for scaling the sideways forces from JET to ITER using Noll's formula.[25] Fig. 5(a) shows the peak amplitude of the expected F_x^{Noll} force in ITER (for $I_{pl}^{ITER} = 15$ MA). Because of the noise and oscillations in signal for the Noll force, the momentary value significantly exceeds the design guidance. For better selection of representative shots, the impulse of the force was calculated and presented in Fig. 5(b). This eliminates the effect of noise and oscillations. The two most representative shots (38070 and 39055) lead to a F_x^{Noll} estimate $\simeq$60 MN. The red colored shots (38705 and 39207) would correspond to $I_{pl}^{ITER} > 15$ MA and can be ignored.

This scan has essentially confirmed the validity of the earlier estimates of F_x^{ITER} based on Eqs. (22) and (23) and a limited number of JET shots, including 38070. The ITER design guidance was supported later by additional measurements[28] and simulations of the currents in the ITER vessel.[29]

B. Sideway forces in kink mode theory

The kink mode theory expresses the sideways force in terms of the real plasma displacement ξ_{11} and for a circular plasma inside the conformal wall gives

$$F_x^{theory} = \pi B_\phi I_{pl} \frac{1 - \frac{\lambda}{q}}{1 - \lambda}(1 - q_a)\xi_{11}, \quad \lambda = \frac{a^2}{a_w^2}, \tag{24}$$

which describes correctly stability of the $m/n = 1/1$ mode but looks different from the Noll formula.

In fact, the real difference is not significant. It is important to keep in mind that the magnetically reconstructed plasma displacement δz_{11} can be significantly different from the real plasma deformation ξ_{11}

$$\delta z_{11} \equiv \frac{M_{IZ,\phi+\pi} - M_{IZ,\phi}}{2I_{pl}} = \frac{1 - q_a}{1 - \lambda}\xi_{11}. \tag{25}$$

The difference is attributed to the presence of the surface currents which screen the real perturbation from the measurements. When expressed in terms of δz_{11}, the theory based formula is similar to the Noll formula

$$F_x^{theory} = \pi B_\phi I_{pl}\left(1 - \frac{\lambda}{q_a}\right)\delta z = \left(1 - \frac{\lambda}{q_a}\right)F_x^{Noll}. \tag{26}$$

The factor $1 - \lambda/q_a$, which takes into account the presence of the eddy currents in the wall, is always less than unity. The value of λ can be determined only by numerical simulations. This, the theory of the kink mode justifies the Noll formula for F_x as the upper estimate of the sideways force and its scaling from JET to ITER.

At the same time, a warning is issued that the surface currents during instabilities make magnetic reconstruction in its present form questionable (e.g., $\delta z \neq \xi_{11}$).

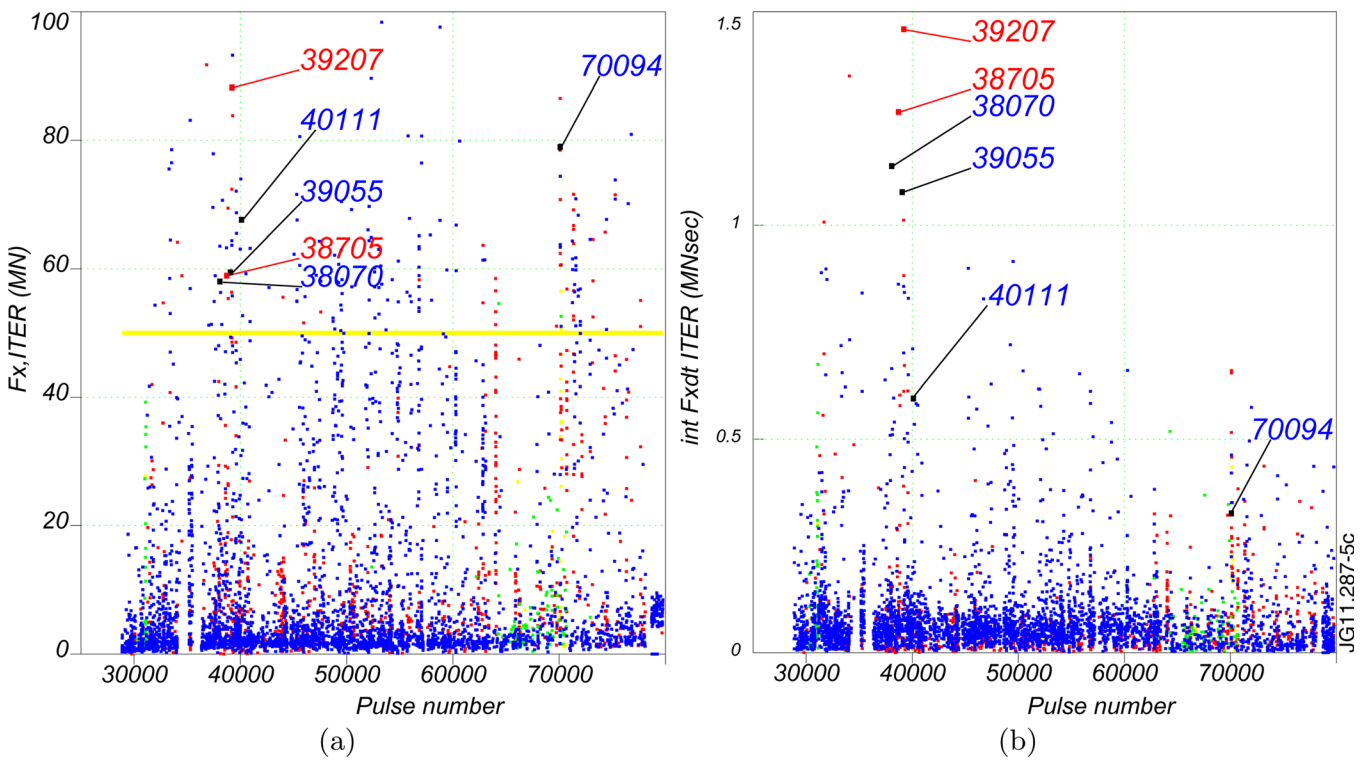

FIG. 5. Sideways forces from all JET disruptions scaled to ITER using Noll's formula vs shot numbers: (a) peak values of sideways forces and (b) impulse $\int F_x^{ITER} dt^{JET}$.

C. Mode rotation is a challenge for interpretation

Of course, not only forces, but also their localization, duration (impulse) and time behavior are important for the vessel structure. In this regard, too many things depend on specific plasma wall-interactions and there is neither sufficient understanding of their physics nor appropriate scalings.

One of the challenges, deserving attention, is represented by toroidal rotation of the mode (and forces),[30] which in ITER can potentially interfere with the eigen-frequencies of the vacuum vessel. The 4 full sets of magnetic diagnostics on JET allow extracting reliable information about mode azimuthal motion during disruptions.

For 4 characteristic VDE shots, the traces of the tip of vectors

$$\delta\vec{M}_{IZ}(t) \equiv \delta M_{51}(t)\vec{\mathbf{e}}_x + \delta M_{73}(t)\vec{\mathbf{e}}_y,$$
$$\delta\vec{I}_{pl}(t) \equiv \delta I_{51}(t)\vec{\mathbf{e}}_x + \delta I_{73}(t)\vec{\mathbf{e}}_y \quad (27)$$

are shown in Fig. 6 as and lines correspondingly, started initially in black. Reversed (Figs. 6(a) and 6(b)) and partial (Fig. 6(c)) rotations represent typical behavior, while there are a few cases with relatively fast regular rotation as in Fig. 6(d) (but with a moderate level of sideways forces).

Such a sporadic behavior indicates that the kink mode rotation is not a core related effect. The boundary physics, probably specific for every disruption, is crucial, which makes the development of the theory of rotation practically impossible. At the same time, a much more modest step, i.e., the understanding of the cause of rotational and sporadic azimuthal behaviors seems to be realistic and important for the next step machines.

V. NEW TYPES OF MHD EQUILIBRIA AND OF MODE COUPLING

In the same way as eddy currents in the shell can provide the saturation of the FBKM in Fig. 3, the Hiro currents can provide the equilibrium of the wall touching kink mode. The difference is that they can stop the plasma motion even by a surface composed of conducting, but mutually insulated tiles.

A. 2-D case with a tile surface conformal to the plasma

Fig. 7 shows the results of WTKM simulations preformed with the present 2-D version of DSC. In this case, a tile covered surface is situated between the plasma and the wall as in Fig. 3. In simulations, it is assumed that the tile surface is transparent to the magnetic field unless the plasma touches the tiles. After touching, the tiles in the wetting zone are assumed to be electrically connected, thus, allowing large Hiro current excitation along the tile surface. The gap between the tile surface and the outer wall is intentionally chosen larger than the gap between the plasma and the wall in the saturated FBKM (Fig. 3(c)).

Before touching tiles, the WTKM instability behaves as a FBKM in a fast regime. The fast MHD regime continues even after initial touching. Because of the fast time scale, it is assumed that the wetting zone becomes ideally conducting for Hiro currents. At this stage, the plasma penetration through the tile surface is negligible (Fig. 7(b)). At this stage, the plasma adjusts its shape to the equilibrium conditions (Fig. 7(c)) with the plasma edge conformal the tile surface in the wetting zone.

In the resulting equilibrium

- the surface currents together with the Hiro currents provide the plasma core equilibrium (in these calculations, the eddy currents in the outer wall also contribute to equilibrium);
- the positive surface currents along the free plasma surface are distributed uniformly, flow along the field lines and are force-free; and
- the force $\vec{i}^{Hiro} \times \vec{B}$, acting on Hiro currents, is applied to the tile surface.

This new type of equilibrium, maintained by the Hiro currents, is in a quasi-stationary evolution regime. Because of finite resistivity of the plasma edge, tiles, and contact resistivity (with potentially very complicated plasma-material interactions physics), the Hiro currents have the tendency to decay and are maintained at the necessary level for equilibrium by the plasma motion into the tile surface. Unlike the hydrodynamics of salt water flow in a pipe, the plasma has no restrictions on its motion to the wall and its flow to the wall

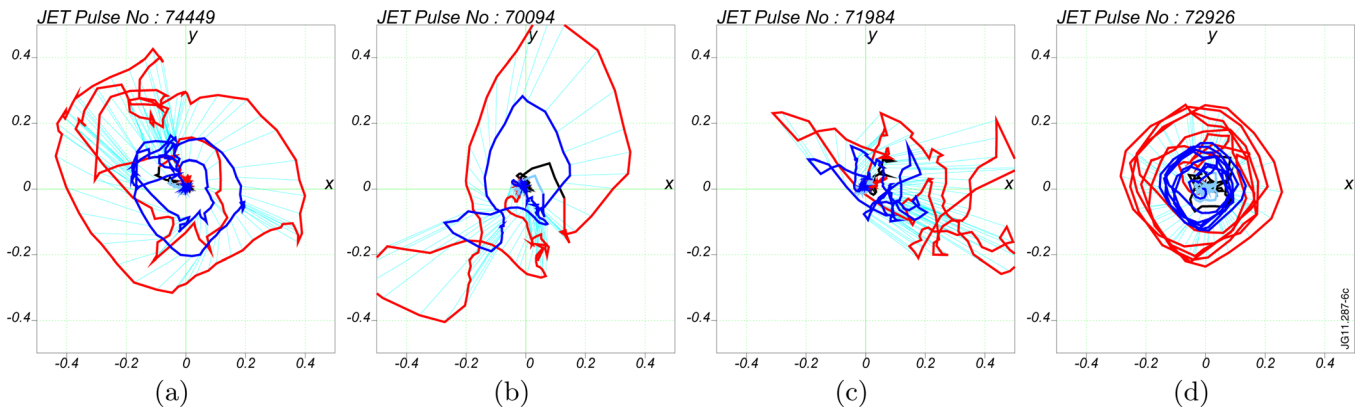

FIG. 6. JET top view on trajectories of the tip of vectors of asymmetries in $\delta\vec{M}_{IZ}$, MA·m and $\delta\vec{I}_{pl}$, MA. (a) Reversed rotation of the mode; (b) Figure 8 azimuth motion with reversal; and (c) azimuthally trapped motion; (d) fast rotation of the mode.

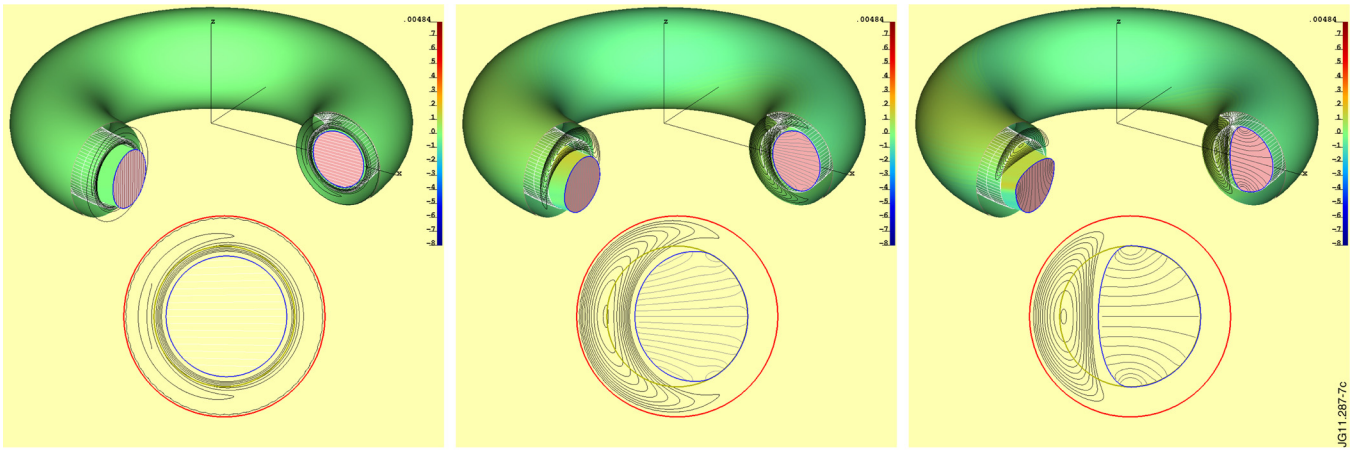

(a) (b) (c)

FIG. 7. Fast regime of the WTKM inside the tile surface. (a) Initially perturbed plasma; (b) fast phase of plasma shape adjustment after touching and excitation of Hiro currents; and (c) saturation of WTKM due to Hiro currents.

$$V_{normal} \neq 0 \tag{28}$$

is automatically adjusted to equilibrium and Hiro current excitation requirements.

This process neutralizes the incoming plasma ions and as a result the plasma loses particles and its cross-section shrinks. Fig. 8 shows several stages of the self-consistent plasma decay and termination. The presented combination of a tile and wall surfaces mimics the real in-vessel environment of tokamaks, where the plasma facing tile surfaces are physically close to the plasma. At the same time, the electromagnetically equivalent conducting wall structure is situated at some distance from its physical location due to ribs, gap, windows, penetrations, etc.

Note, that two regimes shown in Figs. 7 and 8 with (a) generation of the Hiro currents, and (b) plasma decay cannot be reproduced by existing 3-D codes (M3D (Ref. 31) or NIMROD (Ref. 32)) because of their irrelevant to the tokamak plasma boundary condition $V_{normal} = 0$,[33] motivated numerically for the "highly resistive plasma" replacing the vacuum region. Even the resistive evolution of the saturated FBKM in Fig. 3(c) (which initially is not sensitive to the substitution of the vacuum region in these codes) would require elimination of the artificial limitation on V_{normal}: after resistive drifting toward the wall, the FBKM instability will be converted into WTKM and will enter the Hiro current decay regime as in Fig. 8. In reality, plasma touches the walls right in the beginning of disruptions, thus, leaving no room for applications for hydrodynamic models with $V_{normal} = 0$.

B. 3-D equilibria with a localized wetting zone

This kind of equilibrium was already explained in Ref. 17. For the case with $q_a < 1$, the example with a prescribed surface current flow function $I^{surf}(\omega, \phi)$

$$i^s(\omega, \phi) = -\frac{1}{a} I'^{surf}_{\omega} \mathbf{e}_\phi + \frac{1}{R} I'^{surf}_{\omega} \mathbf{e}_\phi, \tag{29}$$

where $i^s = i^{surf}$ on the free plasma surface and $i^s = i^{Hiro}$ in the wetting zone, is shown in Fig. 9(a). In this equilibrium, as in the previous 2-D case, the force is applied to the wall structure, while the surface currents are force free. This may

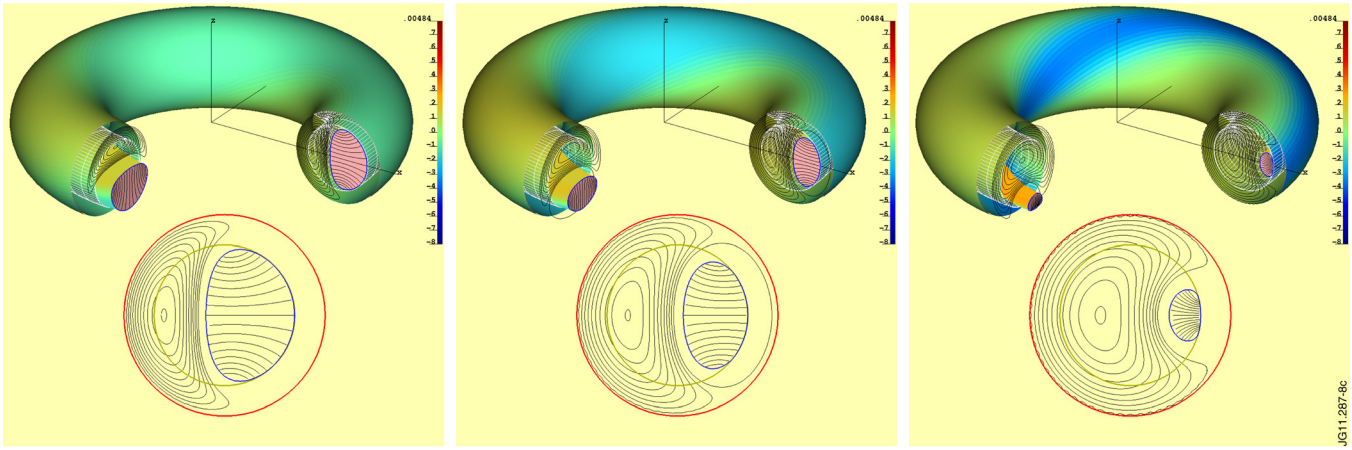

(a) (b) (c)

FIG. 8. Self-consistent plasma/(Hiro currents) decay with plasma moving into the wall. (a) Initial phase of decay; (b) intermediate phase of decay; and (c) final phase of plasma termination.

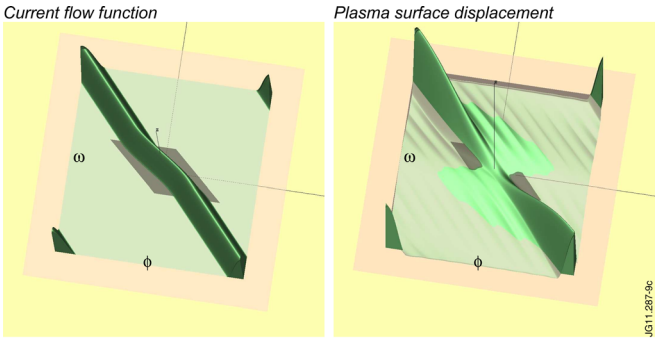

FIG. 9. Flow function of edge currents and the plasma displacement shown on $\phi - \omega$ plane for an example of a 3-D equilibria with $q_a = 0.95$ and a uniform core current density. The wetting zone is shown in a dark grey color. (a) Flow function $I^{surf}(\omega, \phi)$ and (b) plasma surface displacement $\xi(\omega, \phi)$.

explain the relatively long (with respect to MHD time scales) duration (20–25 ms) of the WTKM in VDE on JET.

The important difference with the 2-D case is that the i^{surf} at the plasma surface are not uniform in the poloidal direction. Therefore, they are not in equilibrium along the plasma surface (in the perpendicular direction to the filed lines). The theory of evolution of such a current distribution, which is self-consistently maintained by the driving kink mode, has to be developed. In analogy with the reconnection events, this may lead to time scales, like $\sqrt{\tau_{MHD}\tau_{res}^{edge}}$, which are intermediate between the fast MHD τ_{MHD} and slower plasma edge resistive τ_{res}^{edge} time scales, rather than to a resistive rate of the Hiro currents decay.

C. Mode coupling associated with WTKM

The flow function $I^{surf}(\omega, \phi)$ of the surface current is related to the plasma boundary perturbation $\xi(a, \omega, \phi)$ by equilibrium equations. For the case shown in Fig. 9(a), the displacement $\xi(a, \omega, \phi)$ in Fig. 9(b) was generated using linearized equilibrium equations. The important fact is that $\xi(a, \omega, \phi)$ contains a much broader Fourier spectrum of harmonics than the current flow function or the driving mode itself.

The general conclusion is that even a single helicity driving WTKM leads to excitation of a broad spectrum of plasma boundary displacements, which are translated to the plasma core MHD perturbations $\xi(\rho, \omega, \phi)$. Accordingly, the spectrum of magnetic perturbations $\tilde{B}_\rho(\rho, \omega, \phi) = \vec{B} \cdot \nabla \xi(\rho, \omega, \phi)$ is broad and can cause the destruction of confinement in the core.

This new type of mode coupling makes WKTM a candidate for explanation of the fast destruction of core confinement at the early stage of conventional (non-VDE) disruptions leading to a thermal quench. At the same time, the well-known toroidal mode coupling of FBKM modes would produce only a splitting of a number of separated resonance magnetic surfaces without drastic reduction of confinement.

An intentionally excited WTKM during the current quench may prevent confinement and generation of runaway electrons by their core confinement destruction.

Potential relation of WTKM to the thermal quench and application for suppression of runaway electrons motivate the active experiments on studies of the physics of the WTKM.

VI. DSC

In addition to the physics of disruption, progress was made also in understanding the situation with numerical simulations. As already mentioned in Sec. V, all existing 3-D MHD codes (M3D, NIMROD included) use the boundary condition at the wall $V_{normal} = 0$, which is appropriate for liquid metal or salt water MHD flow in a pipe but not for a tokamak plasma. At the wall, ions are simply converted into neutrals, which no longer participate in the plasma dynamics. Also it is not evident that the essentially hydrodynamic numerical schemes of these codes would ever allow elimination of this restrictive condition affecting the entire macroscopic plasma MHD. As a result, the codes have missed the dominant effect in disruption, i.e., the big Hiro currents in the wall driven by the plasma motion into the wall. Since 2007, when the issue was raised, the boundary condition in M3D and NIMROD remains uncorrected,[31] thus, leaving these codes questionable for disruption simulations.

It is clear that new numerical approaches should be developed with understanding that MHD is only a part of disruption physics. Plasma edge physics and plasma-wall interactions are an intrinsic part of disruptions in tokamaks and the MHD numerical schemes should be suitable for interfacing with this physics. In addition, for proper description of energetic-particle confinement and losses, the plasma core numerical model should be consistent with anisotropy of the high-temperature tokamak plasma.

The new disruption simulation code DSC, which is under development in collaboration between FAR-TECH, Inc (San Diego, CA) and PPPL (Princeton) under a DoE SBIR grant, was already used for illustrations in this paper. At this stage, the single helicity 2-D version of the code is operational.

The code is based on a free boundary plasma model with no restrictions on plasma velocity into the wall, as is shown in Fig. 8. No numerical substitution of vacuum by a "fake" plasma is used and the vacuum field is calculated directly either by solving Maxwell's equations or by using the Greens functions.

The adaptive grids used for the plasma core and explicit plasma-vacuum separation allow accurately resolving the moving plasma boundary. A meshless, "cloud of points" algorithm[34] is one of the innovative methods used for distributing computational grids.

The choice of a coordinate system for adaptive schemes is of highest priority. In the 2-D case, the magnetic field has a poloidal flux function, which determines magnetic surfaces. They can be used as a basis for the computational grid. Introduction of 3-D perturbations destroys the magnetic surfaces and makes the straightforward 2-D approach invalid. With understanding, the 3-D version of DSC will use the so-called reference magnetic coordinates (RMC) $\hat{\rho}, \hat{\theta}, \hat{\zeta}$, in which the magnetic vector potential $\vec{A}$ has the simplest possible form

$$\vec{A} = \bar{\Phi}(\hat{\rho})\nabla\hat{\theta} + \bar{\Psi}(\hat{\rho})\nabla\hat{\zeta} + \bar{\psi}^*(\hat{\rho}, \hat{\theta}, \hat{\zeta})\nabla\hat{\zeta}. \quad (30)$$

Here $2\pi\bar{\Phi}(\hat{\rho}), 2\pi\bar{\Psi}(\hat{\rho})$ represent the toroidal and poloidal magnetic fluxes through the toroidal surface $\hat{\rho} = \text{const}$, while the 3-D function $\bar{\psi}^*(\hat{\rho}, \hat{\theta}, \hat{\zeta})$ contains only resonant Fourier harmonics of the angle variables. RMC are simple

nested toroidal coordinates with the best possible alignment to the 3-D magnetic field.

Introduction of RMC resolves the long standing problem of 3-D coordinates for ergodic magnetic fields, remaining unsolved in stellarator theory.

Relaxing the time step requirements in MHD simulations, which are difficult for parallelization, is another requirement for DSC. In the existing 3-D codes, the time step is typically limited by the fast magneto-sonic waves (Courant condition) which play no role in disruption dynamics. The use of RMC partially resolves the problem of optimization of the time step.

In 1973, Kadomtsev and Pogutse[35] gave an example of how to eliminate the magneto-sonic wave restriction on the time step. The reduced MHD model originated from their publication. In fact, the Kadomtsev-Pogutse approach can be extended to a general 3-D case with toroidal field larger than the poloidal one. In examples of this paper, this type of algorithm was used in DSC for 2-D simulations. It makes the time step determined by a leading instability, rather than by stable waves, and is expandable to the 3-D dynamics.

The integration of MHD with the edge and wall physics is the primary extension of DSC. In this regard, the typical theoretical and computational models of a smooth continuous wall are not applicable for the plasma dynamics. The galvanic plasma-wall contact requires more realistic wall models. At present, the triangle based electromagnetic model of the thin wall was developed. As an important property, it has no singularities in magnetic fields and allows calculating them at the wall surface. This is absolutely necessary for simulation of the plasma-wall contact in the wetting zone as well as for reproduction of the signals from the local magnetic probes during disruptions.

Figs. 10(a) and 10(b) show an example of a simulation by the Cbshl code of calculations of eddy currents excited in the copper shell by an external equilibrium coil of the Lithium Tokamak Experiment (LTX) tokamak. The color expresses the local amplitude of the eddy current stream function. The same model will be used for the ITER plasma facing surface (Fig. 10(c)) in disruption Hiro current simulations.

Four innovative elements, necessary for disruption simulations, distinguish DSC development from existing (essentially invalid) 3-D approaches: (a) free boundary plasma model with no restrictions on V_{normal}, (b) RMC based adaptive grid numerical scheme for the core, (c) time step determined by the leading instability, and (d) a realistic electrodynamic wall model.

VII. DO HALO CURRENTS PLAY A ROLE IN DISRUPTIONS?

The interpretation of currents to the surface of the tiles as the halo currents along the open field lines reflects the fact that these currents are observed far away from the core plasma contact zone with the tiles as in Fig. 10(a).[8] Widely accepted, the same halo current interpretation, applied to the clean case of toroidal asymmetry in the plasma current measurements on JET, has failed even in explaining the sign of the observed effect. Instead, the experimental measurements are consistent with the Hiro currents.

Hiro currents are not the halo currents and are generated along the plasma facing surface. For the 2-D case, they even do not need entry-exit ("source-sink") points. Therefore, the existence of Hiro currents does not exclude the halo current interpretation of the currents to the tile surface, which we will explicitly refer here as Evans currents.[10] Still there several other reasons, why the halo current interpretation, attractive in its simplicity, has no solid ground.

The use of equilibrium reconstruction for instability analysis is not straightforward. As it was shown in Sec. IV, the magnetically reconstructed plasma deformation is different from the real deformation because of the presence of surface and Hiro currents. Equation (25) quantifies this for the $m/n = 1/1$ kink mode. The same statement is valid for the vertical instability. The equilibrium reconstruction also does not take into account the evolutionary connection of different stages of instability and therefore misses the plasma surface currents and Hiro currents (in DIII-D reconstruction the short poloidal connection of halo currents through the wall structure was used instead). The plasma physics of the open field

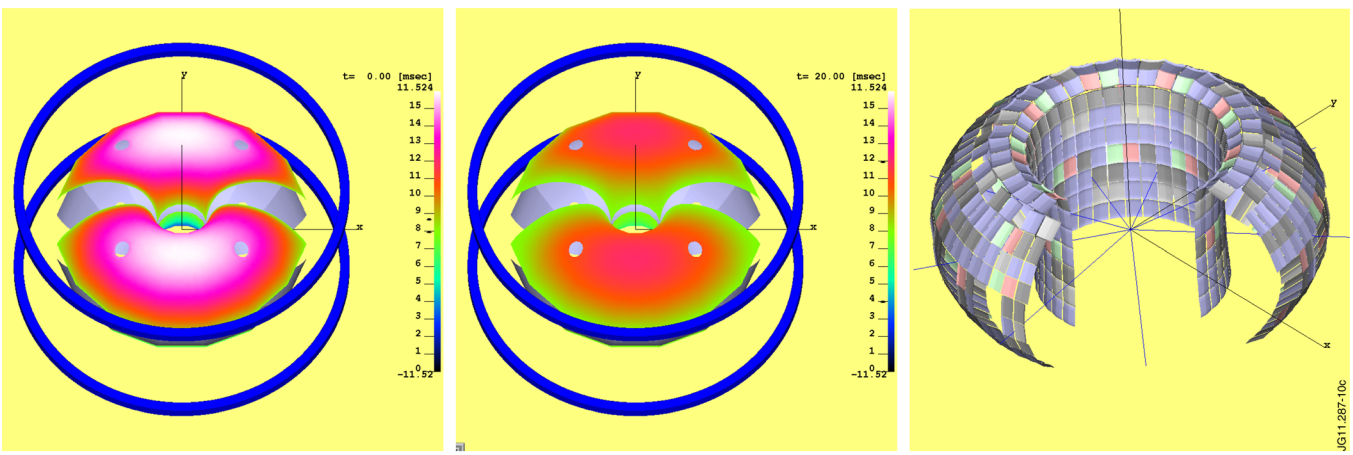

FIG. 10. The computational model of the plasma facing conducting surfaces in LTX and ITER. (a) Eddy currents, generated in the copper shell and an equilibrium coil in LTX, at $t = 0$; (b) decayed eddy current at $t = 20$ ms; and (c) ITER plasma facing Be tile surfaces for Hiro current simulations.

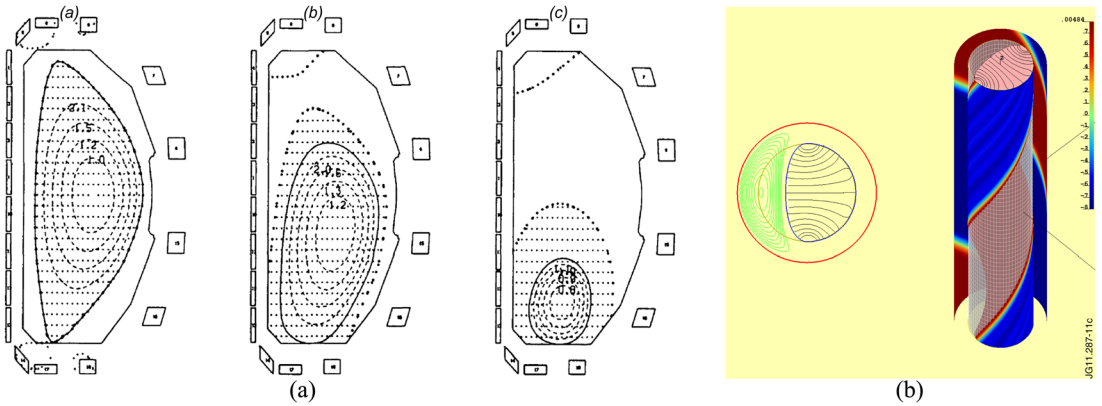

FIG. 11. Two different possibilities for the currents into the tile surface. (a) Three phases of VDE in DIII-D reconstructed using EFIT with the halo area and the halo currents (the plot was reproduced with permission from Ref. 8, Nucl. Fusion **31**, 527 (1991), Copyright © 1991 Institute of Physics: *"Fig. 3. Equilibrium flux plots from EFIT at three times during the vertical instability: (a) 2660 ms (b) 2675 ms, and (c) 2684 ms. Plasma current was allowed in the hatched region, including part of the SOL."*) and (b) wide wetting zone of the $m/n = 1/1$ WTKM equilibrium maintained by the Hiro currents.

line, which should clearly answer the question about electric current carriers on the open field lines, is absent. In numerical simulations, this entire issue is put aside by a hand-made prescription of the media resistivity.

On the other hand, at least, for the kink mode $m/n = 1/1$, the theory of WTKM leaves no place for the halo currents. Fig. 11(b) shows that the plasma-tile contact zone is wide because the plasma adjusts its shape to be conformal to the conducting surface in the wetting zone. As a result of magnetic flux conservation, the wetting zone is much broader than it would be expected based on naive use of an undeformed plasma shape.

The WTKM theory allows currents flowing into the tile surface. Currents are the edge plasma currents and represent the *positive* components of the surface currents coming from the free plasma surface to the tiles. These Evans currents, along with Hiro currents, are also generated by instability. They do not affect the equilibrium and after entering the wetting zone will flow mostly along the field lines in the direction of the plasma current. Still their amplitude in the wetting zone cannot compensate the amplitude of Hiro currents which are always bigger.

The physics of Hiro and Evans currents is different from the physics of halo currents and summarized in the Table I.

Thus, there are many reasons to suspect that the presently accepted role of halo currents in disruption instability is probably the result of misinterpretation. Instead, based on kink mode simulations, the theory of WTKM suggests a different interpretation:

- Transient equilibrium in VDE has a leading plasma edge conformal to the tile surface. It is maintained by negative Hiro currents flowing parallel to the tile surface.
- The tiles measure the positive, concentrated force-free Evans currents from the free plasma surface, rather than the diffused "halo" currents.

The presence of an initial normal magnetic field to the wall surface during vertical instability distinguishes the $n = 0$ VDE from the kink mode. Additional simulations are necessary for a better judgment of potential importance of this difference.

In conclusion, we recall the meaning of different current notions used in this paper: *(a) surface currents* at the plasma boundary generated by free boundary MHD instabilities; *(b) eddy currents* in the wall, excited by perturbed magnetic field, which is screened by the plasma surface currents; *(c) Hiro currents*, which are the negative component of the surface currents shared between plasma and the wall; *(d) Evans currents*, which are the positive component of the surface currents potentially shared between plasma and the wall; *(e) halo currents*, which are the positive diffused currents to the tile surface from outside the last closed magnetic surface (can be confused with the Evans currents).

TABLE I. Currents shared between a plasma and the wall during disruptions.

	Hiro currents	Evans currents:	Halo currents:
1	Both result from magnetic flux conservation.		Derived from questionable use of equilibrium reconstruction. No strong reason for existence.
2	Driven by instability acting as current generator.	Driven by instability acting as voltage generator.	Assumed to be driven by a residual voltage outside the last closed magnetic surface.
3	Highly concentrated at the plasma edge.		Diffused in space with open field lines.
4	Big in amplitude, proportional to plasma deformation.		Limited by the ion saturation current.
5	Absolutely necessary to slow down the instability.	Force-free, little, if any, effect on stabilization.	Secondary, if any, effect on stabilization.
6	**Opposite to I_{pl}.**	**Same direction as I_{pl}.**	**Same direction as I_{pl}.**
7	Consistent with toroidal asymmetry in JET VDEs.		Ruled out as a reason of toroidal asymmetry.

VIII. SUMMARY

Probably, disruptions in tokamaks are too complicated to be completely understood. Still significant progress was made. The new key players, WTKM and Hiro currents, which give a remarkable explanation of the toroidal asymmetry in the plasma current measurements on JET, were identified by theory. The same theory undermined the community wide interpretation of the currents to the plasma facing tiles as the "halo" currents. Instead, the positive component of the surface currents generated by a free boundary instability can enter the tile surface as highly localized Evans currents, introduced by this paper.

The situation with the modeling of disruptions became much more clear. It was realized that all existing 3-D codes have issues with the boundary condition $V_{normal} = 0$ applied to the tokamak plasma dynamics. New approaches for simulation of tokamak MHD suggest (a) implementation of the Shafranov free boundary plasma model, free from the above restriction; (b) transition to adaptive MHD 3-D simulations based on RMC; (c) realistic simulations of in-vessel components; and (d) relaxing the time step requirements. An exact nonlinear analytical solution for the vertical instability has been found. It can be used for benchmarking numerical codes.

The importance of interfacing of the core MHD simulations with the plasma edge and plasma-wall interactions physics is emphasized. Also, theory motivated dedicated experiments (to be described elsewhere) have been suggested for active excitation of the secondary disruptions during the current quench and the Hiro and Evans current measurements on several machines.

Because of the overall complexity of disruptions, the key to plasma stability control is in simplification of the plasma regime without sacrificing performance. The practical approach for solving the disruption problem is in development and implementation of the LiWall Fusion regime,[36] with a simpler core physics than in present tokamaks, the best possible in confinement and stability (no sawteeth, edge localized modes, density limit), with neutral beam injection controlled plasma, and stationary plasma-wall interactions. But this is a separate important topic broader than the disruptions.

ACKNOWLEDGMENTS

This work is partially supported by US DoE Contract No. DE-AC02-09-CH11466. This work was also supported by EURATOM and carried out within the framework of the European Fusion Development Agreement. The views and opinions expressed herein do not necessarily reflect those of the European Commission.

[1]M. A. Leontovich and V. D. Shafranov, in *Plasma Physics and the Problem of Controlled Thermonuclear Reactions*, edited by Acad. M. A. Leontovich (Pergamon, New York, 1961), Vol. 1, p. 255.
[2]V. D. Shafranov, Sov. Phys. Tech. Phys. **15**, 175 (1970).
[3]S. von Goeler, W. Stodiek, and N. Sauthoff, Phys. Rev. Lett. **33**, 1201 (1974).
[4]B. Kadomtsev, Sov. J. Plasma Phys. **1**, 389 (1975).
[5]L. E. Zakharov, Sov. J. Plasma Phys. **7**, 8 (1981).
[6]O. P. Pogutse and E. I. Yurchenko, Nucl. Fusion **18**, 1629 (1978).
[7]E. P. Gorbunov and K. A. Razumova, Atomnaya Energia, **15**, 363 (1963).
[8]E. J. Strait, L. L. Lao, J. L. Luxon, and E. E. Reis, Nucl. Fusion **31**, 527 (1991).
[9]L. L. Lao, H. St. John, R. D. Stambaugh, A. G. Kellman, and W. Pfeiffer, Nucl. Fusion **25**, 1611 (1985).
[10]T. E. Evans, C. J. Lasnier, D. N. Hill, A. W. Leonard, M. E. Fenstermacher, T. W. Petrie, and M. J. Schaffer, J. Nucl. Mater. **220–222**, 235 (1995).
[11]Y. Neyatani, R. Yoshino, and T. Ando, Fusion Technol. **28**, 1634 (1995).
[12]R. S. Granetz, I. H. Hutchinson, J. Sorci, J. H. Irby, B. LaBombard, and D. Gwinn, Nucl. Fusion **36**, 545 (1996).
[13]T. E. Evans, A. G. Kellman, D. A. Humphreys, M. J. Schaffer, P. L. Taylor, D. G. Whyte, T. C. Jernigan, A. W. Hyatt, and R. L. Lee, J. Nucl. Mater. **241–243**, 606 (1997).
[14]N. Pomphrey, J. M. Bialek, and W. Park, Nucl. Fusion **38**, 449 (1998).
[15]R. Litunovski, "The observation of phenomena during plasma disruption and the interpretation of the phenomena from the point of view of the toroidal asymmetry of forces," JET Internal Report Contract No. JQ5/11961, 1995.
[16]P. Noll, P. Andrew, M. Buzio, R. Litunovski, T. Raimondi, V. Riccardo, and M. Verrecchia, in *Proceedings of the 19th Symposium on Fusion Technology, Lisbon*, edited by C. Varandas and F. Serra (Elsevier, Amsterdam, 1996), Vol. 1, p. 751.
[17]L. E. Zakharov, Phys. Plasmas **15**, 062507 (2008).
[18]A. J. Webster, Phys. Plasmas **17**, 110708 (2010).
[19]L. E. Zakharov, Phys. Plasmas **18**, 062503 (2011).
[20]A. J. Webster, Phys. Plasmas **18**, 112507 (2011).
[21]R. R. Khayrutdinovand and V. E. Lukash, J. Comput. Phys. **109**, 193 (1993).
[22]J. B. Lister, V. N. Dokouka, R. R. Khayrutdinov, V. E. Lukash, B. P. Duval, J.-M. Moret, J.-F. Artaud, V. Baziuk, and M. Cavinato, Fusion Eng. Des. **74**, 633 (2005).
[23]S. C. Jardin, N. Pomphrey, and J. DeLucia, J. Comput. Phys. **66**, 481 (1986).
[24]L. E. Zakharov and V. D. Shafranov, in *Reviews of Plasma Physics*, edited by Acad. M. A. Leontovich (Consulant Bureau, New York, 1986), Vol. 11, p. 153.
[25]S. N. Gerasimov, T. C. Hender, M. F. Johnson, L. E. Zakharov, and JET EFDA contributors, in *37th EPS Conference on Plasma Physics Conference Proceedings*, Dublin, Ireland, 21–25 June 2010 (European Physical Society, 2010), P4.121.
[26]V. Riccardo, P. Noll, and S. P. Walker, Nucl. Fusion **40**, 1805 (2000).
[27]V. Riccardo and S. P. Walker, Plasma Phys. Controlled Fusion **42**, 29 (2000).
[28]V. Riccardo, G. Arnoux, P. Beaumont, S. Hacquin, J. Hobirk, D. Howell, A. Huber, E. Joffrin, R. Koslowski, N. Lam, H. Leggate, E. Rachlew, G. Sergienko, A. Stephen, T. Todd, M. Zerbini, R. Delogu, L. Grando, D. Marcuzzi, S. Peruzzo, N. Pomaro, P. Sonato, and JET EFDA Contributors, Nucl. Fusion **49**, 055012 (2009).
[29]C. Bachmann, M. Sugihara, R. Roccella, G. Sannazzaro, Y. Gribov, V. Riccardo, T. C. Hender, S. N. Gerasimov, G. Pautasso, A. Belov, E. Lamzin, M. Roccella, and JET EFDA Contributors. Fusion Eng. Des. **86**, 1915 (2011).
[30]T. C. Hender, G. Arnoux, P. de Vries, S. Gerasimov, A. Huber, M. F. Johnson, R. Koslowski, M. Lehnen, A. Loarte, J. R. Martin-Solís, V. Riccardo, and JET-EFDA Contributors, in EXS/10-3 Proceedings of the 23rd IAEA FEC 2010, Daejeon, Korea, http://www-pub.iaea.org/mtcd/meetings/PDFplus/2010/cn180/cn180_papers/exs_10-3.pdf.
[31]H. R. Strauss, R. Paccagnella, and J. Breslau, Phys. Plasmas, **17**, 082505 (2010).
[32]C. R. Sovinec, A. H. Glasser, T. A. Gianakon, D. C. Barnes, R. A. Nebel, S. E. Kruger, D. D. Schnack, S. J. Plimpton, A. Tarditi, M. S. Chu, and the NIMROD Team, J. Comput. Phys. **195**, 355 (2004).
[33]L. E. Zakharov, Phys. Plasmas **17**, 124703 (2010).
[34]S. A. Galkin, J. E. Grubert, B. P. Cluggish, N. Barov, and J. S. Kim, Rev. Sci. Instrum. **81**, 02B705 (2010).
[35]B. B. Kadomtsev and O. P. Pogutse, Zh. Eksp. Teor. Fiz. **65**, 575 (1973).
[36]L. E. Zakharov, "LiWall fusion the new concept of magnetic fusion," Problems of Atomic Science and Engineering, http://vant.iterru.ru/vant_2011_1.htm, #1 (2011), p. 29.